AIAA JOURNAL
Vol. 43, No. 2, February 2005

# Modeling Pulsed-Blowing Systems for Flow Control

Byung-Hun Kim* and David R. Williams†
*Illinois Institute of Technology, Chicago, Illinois 60616*
Steve Emo‡
*Honeywell Engines, Systems, and Services, South Bend, Indiana 46620*
and
Mukund Acharya§
*Honeywell Engines, Systems, and Services, Phoenix, Arizona 85034*

**A linear model for analyzing the performance of pulsed-blowing actuator systems commonly used in many flow-control applications is presented and compared with experiments. The pulsed-blowing system consists of a regulated air supply, an oscillatory valve, transmission tubing, and an actuator. The elements of the actuator are a cavity and slot at the location in the flow to be controlled. The typical design objective is to achieve the largest possible velocity-fluctuation levels at the actuator-slot exit for a given fluctuating pressure input. However, the performance of the system is strongly dependent on component geometry, flow rate, and frequency of pulsation. Lumped-element models are useful for estimating the performance of the actuator cavity and slot, but fail to account for the effects of the transmission tubing. A distributed model for the tubing combined with a lumped-element model for the actuator provides estimates of the system resonant frequencies and amplitudes. Comparisons with experiments are made for a wide range of tubing lengths, slot widths, mean flow velocities, and forcing frequencies. The resonances of the pulsed blowing system and the changes in resonant behavior are characterized by considering the reflection coefficient of the system. Unexpected behavior such as reversed flow at the slot exit and reduced fluctuation levels with increasing pressure are demonstrated and explained with the system model.**

## Nomenclature

| | | |
|---|---|---|
| $A$ | = | cross-sectional area, $m^2$ |
| $C$ | = | acoustic compliance, $m^3 \cdot s^2/kg$ |
| $c$ | = | adiabatic sonic velocity, m/s |
| $d$ | = | tubing diameter, m |
| $f$ | = | frequency, Hz |
| $G_t$ | = | acoustic series conductance per unit length, $m^3 \cdot s/kg$ |
| $L$ | = | acoustic inertance at actuator, $kg/m^4$ |
| $l$ | = | characteristic length scale, m |
| $l_n$ | = | slot thickness, mm |
| $P$ | = | pressure ($=\bar{P} + p$), Pa |
| $\bar{P}, p$ | = | mean and fluctuating pressure, Pa |
| $P_{\text{abs}}$ | = | absolute mean pressure $=\Delta P_{\text{gage}} + P_{\text{atm}}$, Pa |
| $Q$ | = | total flow rate ($=\bar{Q} + q$), $m^3/s$ |
| $\bar{Q}, q$ | = | mean and fluctuating flow rate, $m^3/s$ |
| $R$ | = | acoustic resistance, $kg/m^4 \cdot s$ |
| $r$ | = | radius, m |
| $St$ | = | Stokes number $=\sqrt{(\omega d^2)/\nu}$ or $\sqrt{(\omega \delta^2)/\nu}$ |
| $U$ | = | velocity ($=\bar{U} + u$), m/s |
| $\bar{U}, u$ | = | mean and fluctuating velocity, m/s |
| $V_o$ | = | actuator cavity volume, $m^3$ |
| $Y$ | = | acoustic shunt admittance, $m^4 \cdot s/kg$ |
| $Z$ | = | acoustic series impedance, $kg/m^4 \cdot s$ |
| $Z_o$ | = | characteristic impedance, $kg/m^4 \cdot s$ |
| $\Gamma$ | = | propagation constant |
| $\gamma$ | = | ratio of specific heats |
| $\Delta f$ | = | frequency difference, Hz |
| $\delta$ | = | slot width, m |
| $\zeta$ | = | reflection coefficient |
| $\kappa$ | = | reduced frequency $=(\omega r/c)$ |
| $\lambda$ | = | wavelength of sound, m |
| $\nu$ | = | kinematic viscosity, $m^2/s$ |
| $\sigma^2$ | = | Prandtl number |
| $\omega$ | = | $2\pi f$, rad/s |
| $\omega_\nu$ | = | characteristic frequency, rad/s |

*Subscripts*

| | | |
|---|---|---|
| act | = | actuator |
| $i$ | = | evaluated at sending end |
| $r$ | = | evaluated at actuator cavity |
| $s$ | = | slot exit |
| $t$ | = | transmission tube estimated per unit length |

*Superscripts*

| | | |
|---|---|---|
| $'$ | = | root mean square |
| $\cdot$ | = | time derivative |

Received 20 April 2004; revision received 26 April 2004; accepted for publication 24 June 2004. 

*Research Associate, Fluid Dynamics Research Center, Mechanical, Materials and Aerospace Engineering Department.
†Professor, Fluid Dynamics Research Center, Mechanical, Materials and Aerospace Engineering Department. Associate Fellow AIAA.
‡Senior Principal Engineer, Development Engineering.
§Senior Principal Engineer.

## I. Introduction

ACTIVE flow control is a focal point of research in the fluid dynamics community, particularly related to aerospace applications. Active flow-control actuators using oscillatory fluid injection through slots or holes on exterior surfaces of aircraft and within aircraft engines have demonstrated the ability to increase component performance. Flow control with oscillatory-type actuators has been used for 1) delay of flow separation around cylinders,[1] 2) stall suppression and lift enhancement on wings,[2–4] 3) mixing enhancement,[5] 4) enhanced lift in helicopter rotor blades, 5) stall suppression in compressor inlets, 6) control of acoustic tones in cavities, and 7) enhancement of vane performance in turbomachinery.

The oscillatory actuators fall into two general classifications, zero-net-mass (also known as synthetic jets) and pulsed-blowing. Synthetic jets are self-contained, with zero net mass addition to the

external flow, whereas pulsed-blowing actuators require a source of pressurized fluid, resulting in a nonzero average flow across the actuator interface.[6] Our research group has been working with the pulsed-blowing type of actuator as a means for improving the performance of compressor vane rows in rotating machinery, and has achieved significant enhancements in compressor vane performance.

However, several challenges are faced in moving the technology from the laboratory setting to an actual engine application. One challenge involves the plumbing associated with connecting a large number of vanes to only a few oscillating valves. The large variation in tubing lengths between the oscillating valve and the actuators produces many resonant frequencies in the system. In addition, the vanes have small passages, which tend to damp oscillations produced by the oscillating valve. Because the objective is to maximize the velocity-fluctuation amplitude at the exit of the actuator, it is often desirable to operate the actuator under resonant conditions. The task of predicting the velocity-fluctuation amplitude that will occur at the exit of an actuator for a given pressure input, oscillating-valve frequency, and system configuration becomes quite difficult.

Recent attempts by other investigators to model the performance of synthetic-jet-type actuators have achieved good success. The devices are small compared to the acoustic wavelengths, which is appropriate for lumped-element modeling. Rathnasingham and Breuer[7] developed a coupled fluid–structure model consisting of five coupled nonlinear first-order differential equations. The system of equations acted as the transfer function to compute the velocity output for a given input to the actuator. McCormick[8] used an electroacoustic (lumped-element) model to predict the performance of a "directed synthetic jet" for use in airfoil separation control. A voice coil was the driver for this particular device. Gallas et al.[9] also used the lumped-element approach to obtain the transfer function for a synthetic jet driven by a lead zirconate titanate (PZT)–diaphragm composite.

The lumped-element analysis uses techniques developed in the 1960s, which simulate acoustic/fluid phenomena in an electric circuit analogy.[10,11] The primary requirement for lumped-element modeling is that the characteristic length scale of the device must be small compared to the acoustic wavelength of the oscillations. Synthetic-jet actuators operating in the kilohertz range need only be smaller than about 100 mm. However, pulsed-blowing actuators may not meet this condition, because the length of tubing between the oscillation-producing valve and the actuator is not small compared to the acoustic wavelength.

For situations in which the actuator's characteristic length and the wavelength of sound are comparable ($1 \sim \lambda$), it is necessary to use a distributed model. Rohmann and Grogan[12] analyzed the dynamics of a pneumatic transmission line with small signals and no mean flow using a distributed model. Using an approach analogous to the electronic transmission line theory, they obtained the constant values of the resistance $R$, inertance $L$, and compliance $C$ for a pipe, assuming rigid walls, negligible end effects, polytropic state changes, and uniformly distributed line elements. Karam and Franke[13] developed a relatively simple distributed model for high-frequency oscillations in tubes with blocked ends based on the line elements developed by Nichols.[14] Iberall[15] already found the same relationships for the line elements, including viscous attenuation and heat-transfer losses in the line. Tijdeman referred to the solutions as low-reduced-frequency solutions, because they are functions of the Stokes number $[=\sqrt{(\omega d^2)/\nu}]$ only, and the solutions are valid for the low-reduced-frequency range ($\kappa \ll 1$ and $\kappa/St \ll 1$). Although Karam and Franke's study with a completely closed end tube was not realistic for many engineering applications, their approach was very successful in predicting resonant frequencies and amplitudes over a range of operating conditions for common aircraft applications, and their study formed the basis for more realistic systems.

The objective of this paper is to simulate the performance of a pulsed-blowing system by combining a lumped-element model for the actuator with a distributed model for the transmission tube. After the experimental setup is described in Sec. II, a model for the system is presented in Sec. III that combines the actuator and the tubing that attempts to predict the transfer function of the fluctuating velocity to input-pressure oscillation. The model predictions are compared to experimental data obtained over a wide range of operating conditions. The resonance of pulsed-blowing systems is characterized with reflection coefficients in Sec. IV. Some nonintuitive phenomena related to actuator performance, such as reversed flows at the actuator exit, are discussed in Sec. V.

## II. Experimental Arrangement

The experiments were conducted with the simplified setup shown in Fig. 1, whose key geometric dimensions simulated an actuator used to control flow separation on a compressor stator vane. The test article consisted of a small cavity built into the testing block with a narrow slot across the span. Unsteady pressures were measured with two Kulite (Model XCS-093) pressure transducers, one located in the actuator cavity and a second transducer located close to the downstream exit of the oscillating valve. Mean line pressures were measured with a Setra Model 239 transducer at the actuator cavity, as shown in Fig. 1. Velocity measurements were made with a hot-wire probe and a Disa Model 55D01 anemometer. The hot-wire sensor was placed at the midspan of the slot, as close to the exit plane as possible. A Speedaire 200 psig regulator set the driving pressure to the system. The mean flow rate was measured with an RCM Industries flow meter, Model $\frac{1}{2}$-71-L-40-I, with a maximum range of 40 standard cubic feet per minute (SCFM).

Four different tube lengths ranging from 0.051 m (2 in.) to $0.914 \pm 0.005$ m (36 in.) were used with a combination of three different actuator slot widths, $0.40 \pm 0.025$ mm (0.016 in.), $0.813 \pm 0.025$ mm (0.032 in.), and $2.16 \pm 0.025$ mm (0.085 in.), to investigate the role of tubing length and slot width in the distributed model. Thus, tubing lengths varied by a factor of 19 and slot widths by a factor of 5. Table 1 shows the experimental parameters used for the combined lumped-element and distributed model. Hot-wire measurements of the mean and rms slot velocity taken along the span of the actuator slot (span = 0.0381 m (1.5 in.)) are shown in Figs. 2a and 2b, respectively. Three different supply-pressure amplitudes are shown, with the forcing frequency at 920 Hz and slot width 2.16 mm (0.085 in.). This configuration had the largest spanwise variation in rms velocity. The rms slot exit velocity shown in Fig. 2b varied by $\pm 2$ m/s at $u'_s = 13$ m/s. Other uncertainties in the experimental measurements are listed in Table 2.

Two different oscillating pressure sources were used over the course of the study. A voice-coil driver was used to produce a zero net mass disturbance for the purpose of measuring the lumped-element parameters of the actuator. A siren valve produced flow oscillation for the experiments on the pulsed-blowing system. The siren valve is a proprietary design constructed by Honeywell, whose frequency is proportional to the speed of a servomotor. The valve used in this experiment had an upper frequency limit of 1400 Hz.

The validity of the pulsed-blowing system model was tested by measuring the transfer functions $p'_r/p'_i$, $u'_s/p'_i$, and $u'_s/p'_r$ using the

**Table 1 Experimental parameters for the simplified experimental setup**

| Parameter | Value |
|---|---|
| Inner tubing diameter, mm | 8.13 (0.32 in.) ± 0.02 |
| Tubing lengths, m | 0.051, 0.140, 0.381, 0.914 ± 0.005 |
| Slot span, cm | 3.8 (1.5 in.) ± 0.01 |
| Slot thickness, mm | 8.0 (0.315 in.) ± 0.01 |
| Slot widths, mm | 0.406, 0.813, 2.16 ± 0.025 |
| Cavity volume, $m^3$ | $1.01 \times 10^{-5} \pm 0.025 \times 10^{-5}$ |

**Table 2 Uncertainty of the experimental measurements**

| Measurement | Uncertainty |
|---|---|
| Hot wire velocity | 20 m/s ± 0.17 m/s |
| Kulite fluctuating pressure | ±0.0016 psi g |
| Static pressure | ±0.0025 psi g |

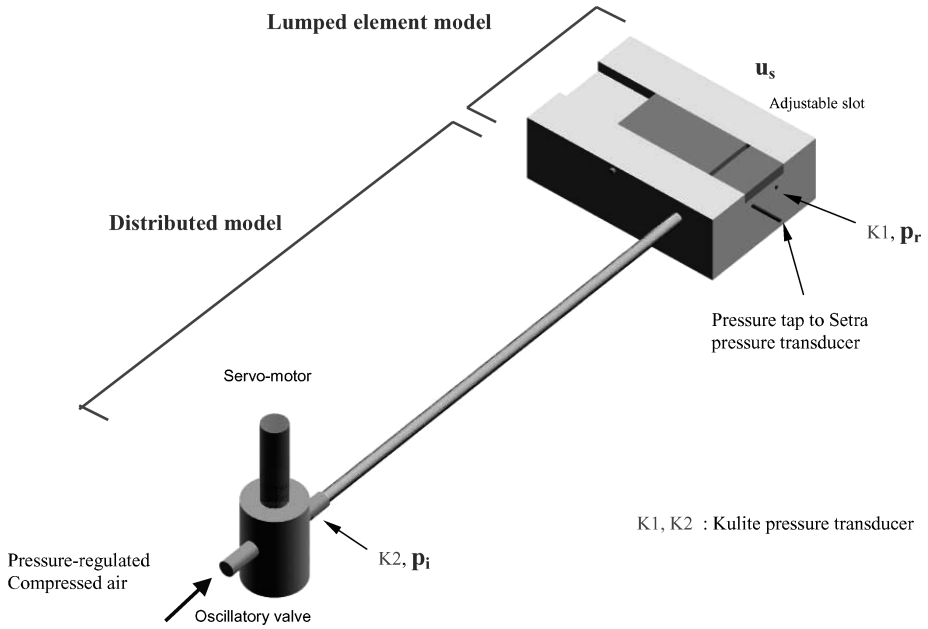


**Fig. 1 Simplified experimental setup for pulsed blowing system study.**

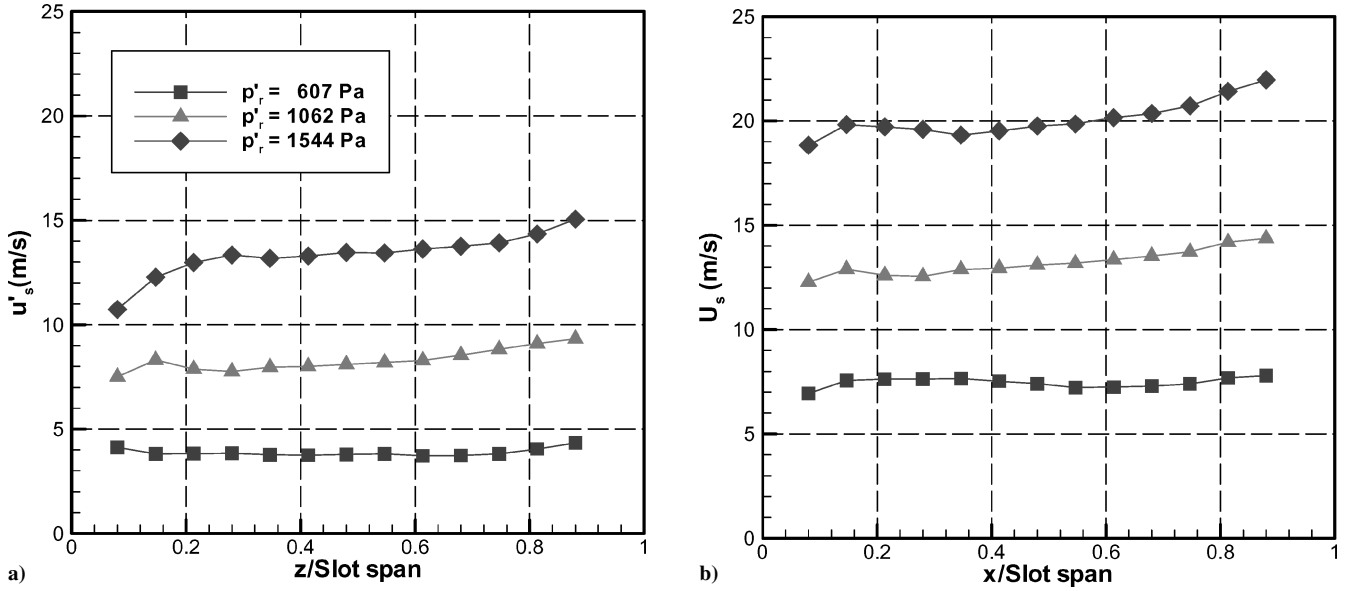


**Fig. 2 Mean and rms velocity measurements along the span of the actuator slot with a slot width of 2.16 mm: a) mean velocity and b) rms velocity at frequency = 920 Hz.**

two Kulite transducers K1 and K2 and a hot-wire probe. The transfer function $p_r'/p_i'$ was obtained from the ratio of the fluctuating pressure measured in the actuator cavity $p_r'$ (K1 pressure transducer) to the inlet pressure $p_i'$ (K2 pressure transducer). The transfer function $u_s'/p_i'$ was obtained from the hot-wire measurement of the fluctuating velocity at the slot exit $u_s'$ and the measurement of the fluctuating pressure $p_i'$ with K2 pressure transducer.

All data were acquired with a PC-based data acquisition system using Labview software and a National Instruments data acquisition card sampling at either 10 or 20 kHz. An Ithaco low-pass filter (Model 4212) was used for antialiasing purposes with a low-pass frequency cutoff of 4 kHz.

## III. Modeling the Pulsed-Blowing System

### A. Lumped Element Model

In typical aircraft compressor applications the pulsed-blowing system will require tubing on the order of a meter in length between the oscillating valves and actuator, and the forcing frequencies will be in the range of hundreds of hertz. Therefore, with centimeter-scale acoustic wavelengths the lumped-element approximation will not be valid for the overall system, and a distributed approach is required for the transmission tubes. On the other hand, the stators and their corresponding actuators are physically much smaller than the wavelength of sound, so the lumped-element model of the actuator can be used as the terminating boundary condition for the transmission tube. The principal modeling elements of the oscillatory flow through the components of the pulsed-blowing system are described below.

Acoustic inertance (mass) is defined by Beranek[10] as a mass of air accelerated by a net force, which acts to displace a gas without appreciably compressing it. Acoustic compliance, on the other hand, is associated with an adiabatic compression process in frictionless flow. They are defined in Eqs. (1a) and (1b):

$$L_{\text{act}} = \rho l / A_s \tag{1a}$$

$$C_{\text{act}} = V_o/\gamma P_{\text{abs}} = V_o \big/ \rho c^2 \tag{1b}$$

$V_o$ is the actuator cavity volume and $l$ is the effective thickness of the actuator slot as shown in the diagram in Fig. 3a. The effective thickness $l$ is $l = l_n + l_c$, where $l_n$ is the actual thickness of the plate and $l_c$ is the mass end correction. Using Ingard's results,[16] the mass end correction for a circular orifice or slot in a flanged plate with $\xi < 0.4$ is approximated by Eq. (2):

$$l_c \cong 0.48 \cdot A_s^{\frac{1}{2}}(1 - 1.25\xi) \tag{2}$$

where $\xi = \delta / W_{\text{plate}}$ ($W_{\text{plate}}$ = width of the plate) for a slot, and $\xi$ goes to zero in the flanged end with a large baffle. Therefore, $\xi$ is negligible in this study, and the end correction is $l_c \approx 0.48 \cdot A_s^{1/2}$. The end correction in Eq. (2) is dependent on only $A_s^{1/2}$ when $\xi$ is very small and is independent of the shape of the apertures.

A schematic of the lumped-element model for the pulsed-blowing system is shown in Fig. 3b following the work of McCormick[8] and Gallas et al.[9] The equivalent circuit consists of an acoustic compliance $C_{\text{act}}$, acoustic inertance $L_{\text{act}}$, and acoustic resistance $R_{\text{act}}$ associated with the flow of air through the actuator slot, and an acoustic inertance $L_{\text{tube}}$ and acoustic resistance $R_{\text{tube}}$ for the tubing. The lumped-element model parameters of the actuator and tubing are listed in Table 3 and are mainly based on the geometry of the stator actuator.

Acoustic resistance is related to the dissipative losses occurring when fluid flows through small slots or orifices. The nonlinear behavior of the quadratic relation between pressure and velocity is important in estimating the acoustic resistance of the flows at high amplitudes.[17–19] Steady flow calibrations of the mean slot velocity as a function of pressure were done for different slot widths. The acoustic resistance of oscillating flows through a slot was assumed to be the same as the steady-flow resistance, so $R_{\text{act}}$ was computed from the measurements of the acoustic resistance $R_{\text{act}}$ for the steady blowing using

$$R_{\text{act}} = \bar{P} / \bar{Q} \tag{3}$$

Figure 4 shows the resistance as a function of slot velocity for three different slot widths.

**Table 3 Lumped-element model parameters corresponding to the experimental parameters in Table 1**

| Parameter | Value |
|---|---|
| $L_{\text{act}}$, kg/m$^4$ | 296 |
| $C_{\text{act}}$, m$^5$/N | $7.11 \times 10^{-11}$ |
| $R_{\text{act}}$, kg/s $\cdot$ m$^4$, at 450 Hz | $3.61 \times 10^5$ |
| $L_{\text{tube}}$, kg/m$^4$ | $3.93 \times 10^3$ |
| $R_{\text{tube}}$, kg/s $\cdot$ m$^4$, at 450 Hz | $8.80 \times 10^4$ |

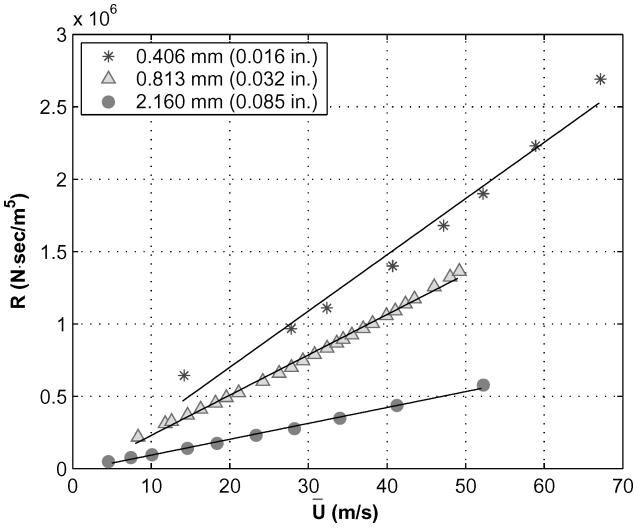


**Fig. 4 Velocity and resistance through the actuator associated with steady blowing for three slot widths.**

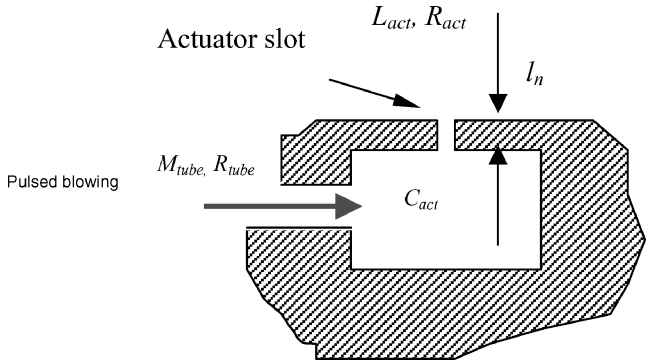


a)

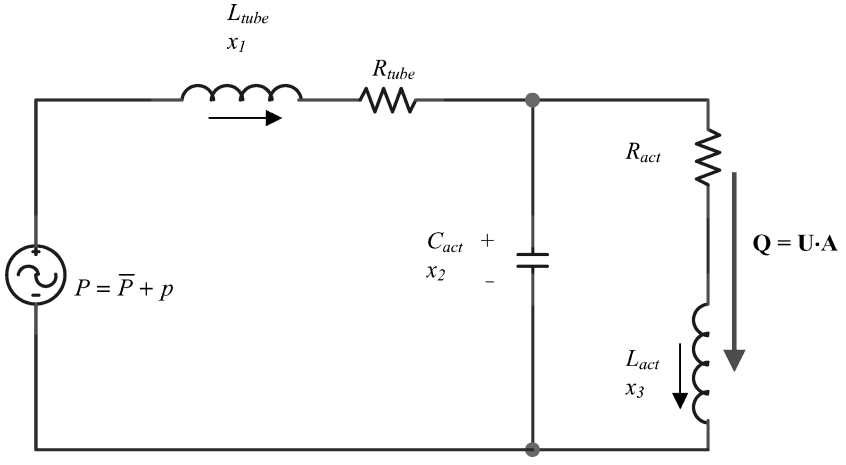


b)

**Fig. 3 Lumped electroacoustic model for a pulsed blowing system: a) actuator diagram and b) equivalent circuit.**

Analogously to the voltage and current in the electric circuit, the instantaneous pressure difference across the inertance $L_{act}$ and the volume flow through the compliance $C_{act}$ can be expressed as

$$p = L_{act}\frac{dq}{dt} \tag{4a}$$

$$q = C_{act}\frac{dp}{dt} \tag{4b}$$

State variables for the lumped elements can be used to model the pulsed blowing system shown in Fig. 3b. A state variable $x_1$ is selected to be the volume flow rate through $L_{tube}$, $x_2$ represents the pressure difference across $C_{act}$, and $x_3$ is the volume flow rate $q$ through $L_{act}$:

$$\dot{x}_1 = (1/L_{tube})(p - R_{tube}x_1 - x_2), \qquad \dot{x}_2 = (1/C_{act})(x_1 - x_3)$$

$$\dot{x}_3 = (1/L_{act})(x_2 - R_{act}x_3), \qquad q = x_3 \tag{5}$$

The single-input $[u(t) = p(t)]$ and single-output $[y(t) = Q(t)]$ system is obtained in Eq. (5) with a three-dimensional state equation where $A$ is a $3 \times 3$ matrix, $B$ is a $3 \times 1$ matrix, and $C$ is a $1 \times 3$ constant matrix:

$$\dot{x}(t) = Ax(t) + Bu(t), \qquad y(t) = Cx(t) \tag{6}$$

$$\begin{bmatrix}\dot{x}_1\\ \dot{x}_2\\ \dot{x}_3\end{bmatrix} = \begin{bmatrix}-\frac{R_{tube}}{L_{tube}} & -\frac{1}{L_{tube}} & 0\\ \frac{1}{C_{act}} & 0 & -\frac{1}{C_{act}}\\ 0 & \frac{1}{L_{act}} & -\frac{R_{act}}{L_{act}}\end{bmatrix}\begin{bmatrix}x_1\\ x_2\\ x_3\end{bmatrix} + \begin{bmatrix}\frac{1}{L_{tube}}\\ 0\\ 0\end{bmatrix}[p]$$

$$q = [0 \quad 0 \quad 1]\begin{bmatrix}x_1\\ x_2\\ x_3\end{bmatrix} \tag{7}$$

Finally, the cross-sectional averaged fluctuating velocity is obtained from the flow rate as

$$u = q/A_s \tag{8}$$

where $A_s$ is the slot cross-sectional area.

Because the pulsed-blowing system was modeled as a third-order system, only one natural frequency of the system exists, which is the Helmholtz resonance mode $[\omega = 1/\sqrt{(L_{act}C_{act})}]$. The Helmholtz resonance frequency was measured to be approximately 1800 Hz with an external flow blowing across the top of the slot to create a resonant tone. The mass end correction $l_c$ was computed from the measured frequency.

A comparison of the predicted slot exit velocity $u'_s$ with the experimental measurements over the frequency range 20–450 Hz is shown in Fig. 5a. In this experiment, a voice-coil driver was used to produce velocity fluctuations with a zero net mass addition, and consequently a zero mean velocity. A time-series signal from the hot-wire anemometer is shown in Fig. 5b before and after derectification. Because the hot-wire sensor was located inside the slot, the mean velocity is actually zero. A monotonic decrease in the rms amplitude of the fluctuating exit velocity occurs with increasing frequency, as shown in Fig. 5a. With a standard deviation in the velocity of 0.6% between the measurement and model, generally good agreement between the model and experiment can be seen over the range of frequencies tested.

### B. Combined Lumped Element Model and Distributed Model

The analysis of the transmission tube shown in Fig. 6 is based on the work of Nichols[14] and Karam and Franke.[13] The infinitesimal segments of the transmission tube can be modeled with lumped elements such as $R_t$, $G_t$, $L_t$, and $C_t$. The basic theory of the transmission line is described by Skilling.[20] Extending the development

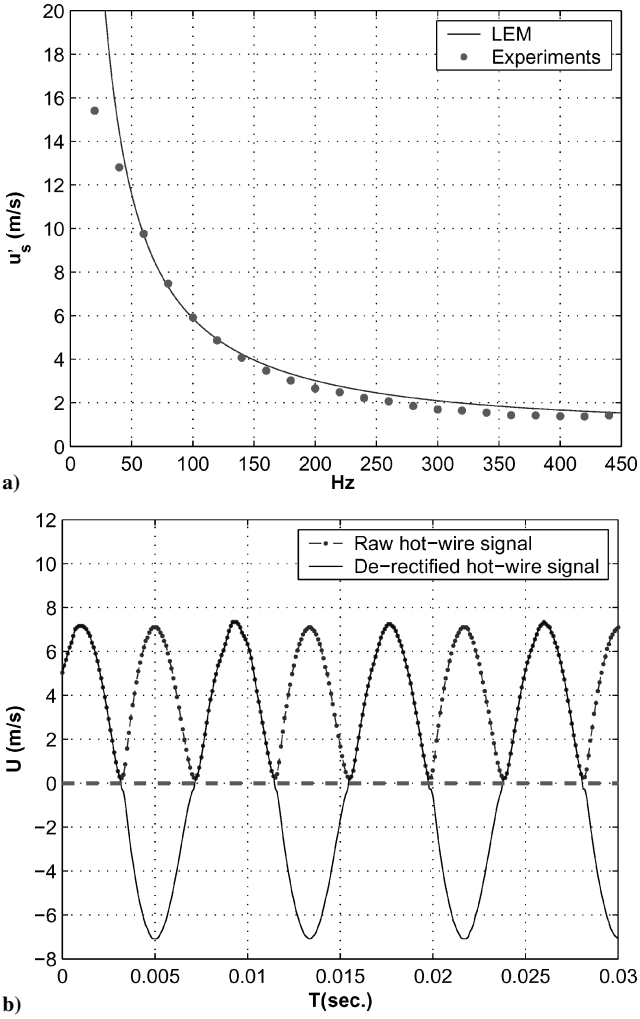


**Fig. 5 Comparison of lumped-element model and experimental measurements of actuator exit velocity: a) rms amplitude dependence on frequency and b) hot-wire time series before and after derectification at 120-Hz frequency.**

of Nichols, Karam and Franke derived simplified relationships for the line elements that are valid in the high-Stokes-number regime ($St \gg \sqrt{8}$). In this study the high-Stokes-number approximations for $R_t$, $G_t$, $L_t$, and $C_t$ are used in Eqs. (9–11). The approximations are based on the exact solution of the two-dimensional, laminar, incompressible, fully developed circular pipe flow driven by the pressure gradients in the quasi-steady state. The Stokes numbers for the oscillating flow through the circular pipe were in the range from 5 to 200, producing reduced frequencies in the range of $0.0035 \le \kappa \le 0.162$. Therefore, the analytic solution of the low-reduced-frequency model[21] chosen here is appropriate.

Following Rohmann and Grogan[12] the fluid oscillations in a cylindrical tube are governed by

$$\frac{dp}{dx} = Z_t q = (R_t + i\omega L_t)q \tag{9}$$

$$\frac{dq}{dx} = Y_t p = (G_t + i\omega C_t)p \tag{10}$$

An important aspect of the analysis is that the series resistance $R_t$ and conductance $G_t$ are frequency-dependent. These quantities are defined as

$$R_t = \tfrac{1}{2}L\sqrt{\omega\omega_v} + 8\pi\mu/A^2 \tag{11}$$

$$G_t = [(\gamma - 1)/2\sigma]C\sqrt{\omega\omega_v} \tag{12}$$

$$L_t = \rho/A \tag{13}$$

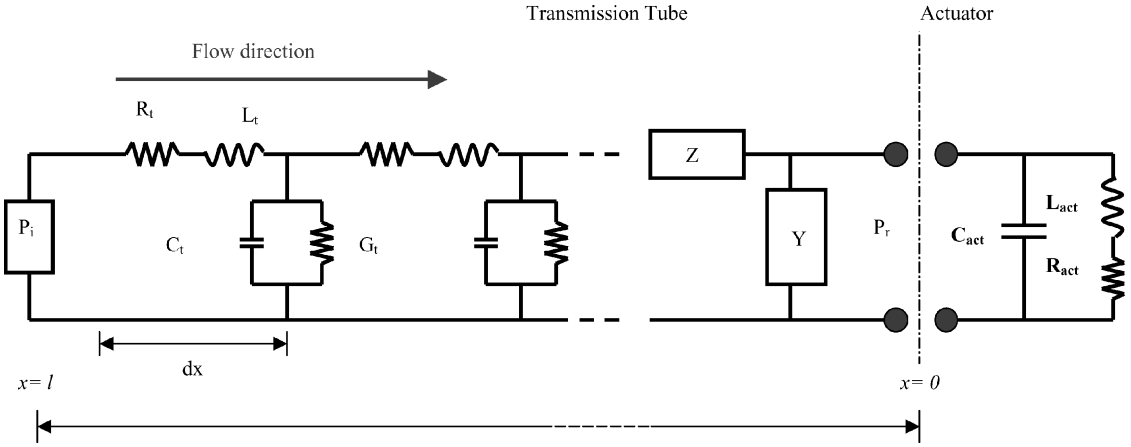


**Fig. 6 Combined lumped-element model for the actuator and distributed model for the transmission tube.**

**Table 4 Distributed and lumped element model parameters estimated at 400 Hz corresponding to the experimental parameters in Table 2[a]**

| Parameter | Value |
|---|---|
| Tubing, per unit length, /m | |
| $L_t$, kg/m$^5$ | $2.31 \times 10^4$ |
| $C_t$, m$^3 \cdot$ s$^2$/kg | $3.63 \times 10^{-10}$ |
| $G_t$, m$^3 \cdot$ s/kg | $1.17 \times 10^{-8}$ |
| $R_t$, kg/m$^5 \cdot$ s | $1.73 \times 10^6$ |
| Stokes number | $5 \sim 200$ |
| Actuator (0.813-mm slot) | |
| $L_{\text{act}}$, kg/m$^4$ | 410 |
| $C_{\text{act}}$, m$^4 \cdot$ s$^2$/kg | $7.057 \times 10^{-11}$ |
| $R_{\text{act}}$, kg/m$^4 \cdot$ s at $\bar{U} = 22$, m/s | $5.39 \times 10^5$ |

[a] $R$ and $G$ are functions of frequency.

$$C_t = A/\gamma P_{\text{abs}} \tag{14}$$

where the characteristic frequency $\omega_v$ is defined as $\omega_v = R_t/L_t = 8\pi\nu/A$. Using Eqs. (11–14), the elements for the transmission tube per unit length can be computed. The specific values used in this experiment are listed in Table 4 based on an oscillation frequency of 400 Hz.

The characteristic impedance $Z_o$ for the transmission tube and the impedance for the actuator $Z_r$ shown in Fig. 3 are determined from the following equations:

$$Z_o = \sqrt{\frac{Z_t}{Y_t}} \tag{15a}$$

$$Z_r = \frac{j\omega L_{\text{act}} + R_{\text{act}}}{1 + j\omega C_{\text{act}} R_{\text{act}} - \omega^2 C_{\text{act}} L_{\text{act}}} \tag{15b}$$

The actuator impedance $Z_r$ is frequency-dependent, which has a strong effect on the dynamic response of the pulsed blowing system. Using Eqs. (9) and (10) with the impedance $Z_r$ and $Z_o$, the transfer function $p_r'/p_i'$ is obtained in closed form as

$$\frac{p_r'}{p_i'} = \left| \frac{\sinh(A + Bj)}{\sinh[(A + \alpha l_t) + j(B + \beta l_t)]} \right| \tag{16}$$

where $\tanh(A + Bj) = Z_r/Z_o$ and the propagation constant $\Gamma = \alpha + \beta j = \sqrt{(Z_t Y_t)}$. The real part of the propagation constant, $\alpha$, is related to the attenuation of the pressure wave transmitted through the tube, and the imaginary part, $\beta$, is related to the phase shift that occurs between the input pressure and actuator pressure waves.

The rms of the fluctuating pressure in the actuator is denoted by

$$p_r' = Z_s q_s', \tag{17}$$

where $q_s'$ is the rms of the fluctuating flow rate through the slot, $q_s' = A_s \cdot u_s'$. $Z_s$is the impedance to oscillating flows through the slot, which is $Z_s = j\omega L_{\text{act}} + R_{\text{act}}$. The acoustic inertance $L_{\text{act}}$ for the slot was estimated in the previous section using Eq. (1a) with the end correction shown in Eq. (2). The acoustic resistance $R_{\text{act}}$ was estimated using the process described by Eq. (3). For example, with a mean slot velocity of 22 m/s the resistance value of $R_{\text{act}} = 5.39 \times 10^5$ kg/m$^4 \cdot$ s was used for a slot width of 0.813 mm.

Therefore, the transfer function $(u_s'/p_i',)$ of the rms fluctuating velocity $u_s'$ at the slot exit to the input inlet rms of the fluctuating pressure $p_i'$, is expressed as

$$u_s'/p_i' = (1/A_s Z_s)(p_r'/p_i') \tag{18}$$

Using Eq. (17), the transfer function $u_s'/p_r'$ is simply denoted as

$$u_s'/p_r' = 1/(A_s \cdot Z_s) \tag{19}$$

## IV. Results

The ability of the linear model to simulate the effect of transmission tubing length on the pulsed-blowing system performance was tested by comparing transfer functions $p_r'/p_i'$ for the pressures across the transmission tubes with different tubing lengths. The results are shown in Figs. 7a–7d for four different tubing lengths, $l_t = 0.0508$ m (2 in.), 0.152 m (6 in.), 0.381 m (15 in.), and 0.914 m (36 in.).

One first notices that the number of resonant peaks increases as the tube length is increased, which is behavior not captured by the lumped-element actuator model alone. Clearly, a distributed model for the transmission tubing should be included in any model of a pulsed-blowing system. In Fig. 7a the measurements for the longest tube ($l_t = 0.914$ m) indicate a change in resonance behavior as the forcing frequency is increased. The combined model predicts the first four resonant frequencies to be $f = 182$, 366, 547, and 722 Hz, which are at approximately the same frequency spacing of $\Delta f = 182$, 184, 181 and 175 Hz. However, unlike the first four peaks, the fifth and sixth peaks at 873 and 987 Hz appear at irregular intervals of $\Delta f = 151$ and 114 Hz. When the forcing frequency exceeds 1000 Hz, the last two peaks appear at 1150 and 1324 Hz with a frequency difference $\Delta f = 174$ Hz, which is slightly smaller than the frequency interval observed at lower frequencies.

The first peak frequencies at 182 Hz in Fig. 7a and 417 Hz in Fig. 7b could be predicted using the simple rule that a tube terminating with an open end resonates when the tubing length matches the half wavelength of the sound. But the data at higher forcing frequencies, such as, the peaks at 820 Hz and 1233 Hz in Fig. 7c and at 1040 Hz at 7d, are not predicted by the simple "open end" rule. The

shift in resonant frequencies that occurs as the forcing frequency is increased indicates that the resonance characteristics of the pulsed-blowing system also depend on the tubing end impedance.

The amplitudes of the resonance peaks also depend on the tube length. Comparing the amplitudes of the first resonant peaks in Figs. 7a–7d, one sees the amplitude steadily increase from $p'_r/p'_i = 0.6$ at $l_t = 0.914$ m (36 in.) to $p'_r/p'_i = 2.2$ at $l_t = 0.051$ m (2 in.) as the tube gets shorter. The amplitude of $p'_r/p'_i$ with $l_t = 0.914$ m (36 in.) is greater than one when the forcing frequency exceeds 1000 Hz, and even with tubing length $l_t = 0.152$ m (6 in.), the second peak reaches $p'_r/p'_i = 3.5$ at 1240 Hz. The amplitude of $p'_r/p'_i > 1$ indicates that the pressure fluctuations in the actuator cavity are greater than the input pressure fluctuations, even though the cross-sectional area of the actuator cavity is much larger than that of the tube.

The effects of the tubing length on the transfer function between the slot exit velocity and input-pressure fluctuations $u'/p'_i$ are shown in the amplitude and phase plots, Figs. 8–10. The shapes of the

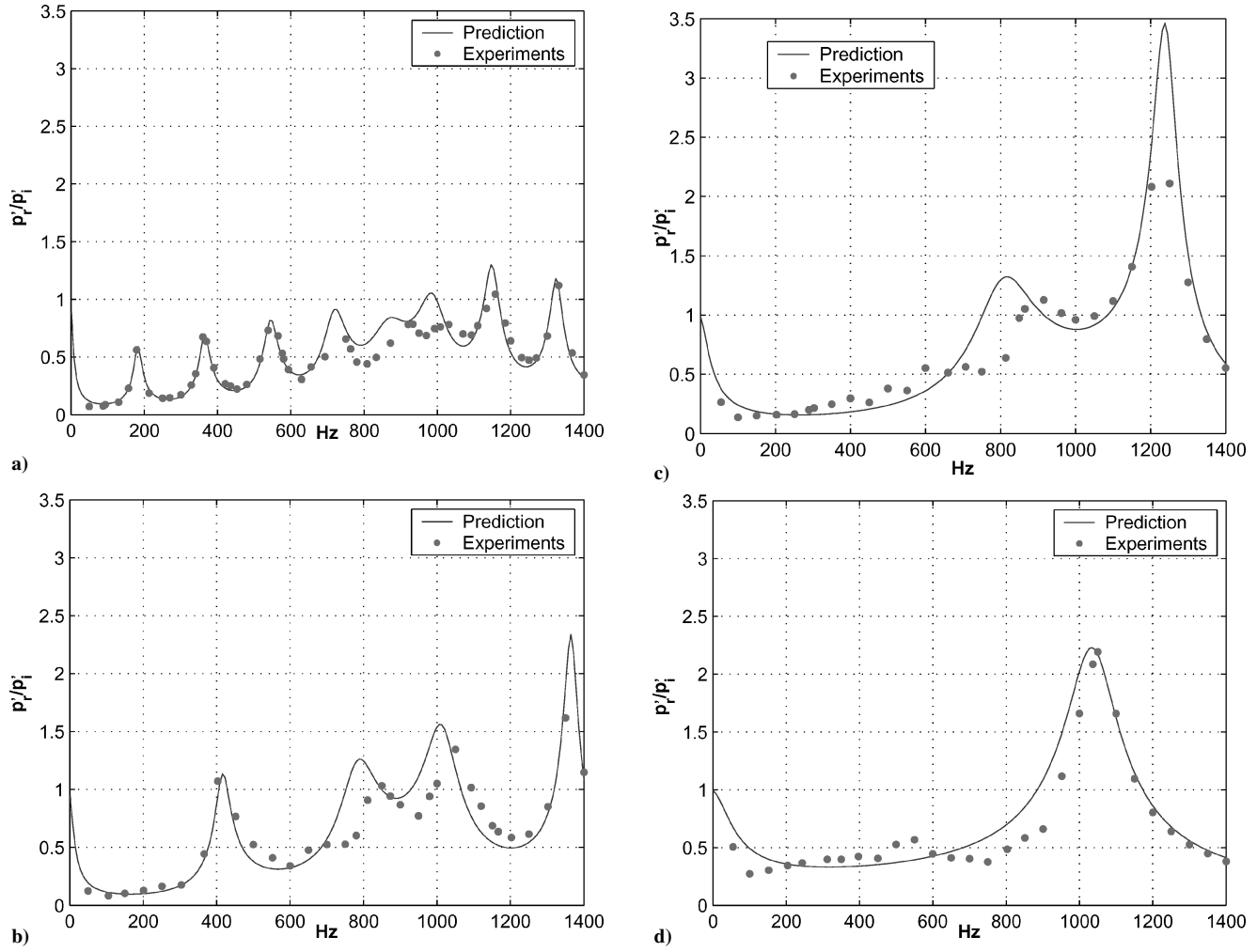


**Fig. 7 Effect of tubing length on $p'_r/p'_i$ in comparison of combined model and experiments with slot width 0.813 mm (0.032 in.): a) $l_t = 0.914$ m (36 in.), b) $l_t = 0.381$ m (15 in.), c) $l_t = 0.152$ m (6 in.), and d) $l_t = 0.051$ m (2 in.).**

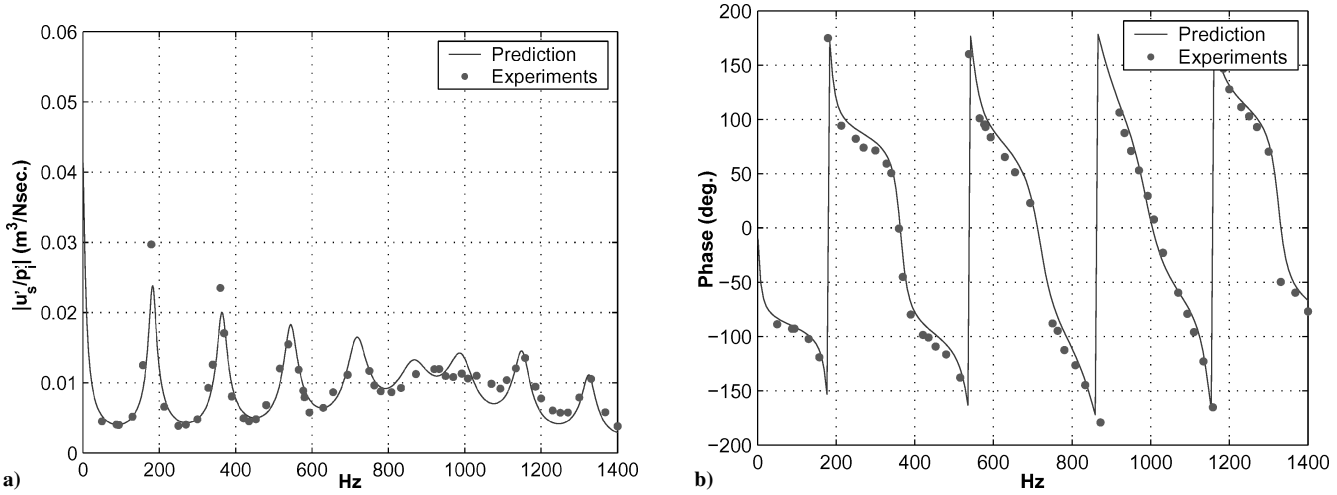


**Fig. 8 Comparison $u'_{ss}/p'_i$ of combined model and experiments with slot width $\delta = 0.813$ mm (0.032 in.) and tubing length $l_t = 0.914$ m (36 in.): a) magnitude and b) phase.**

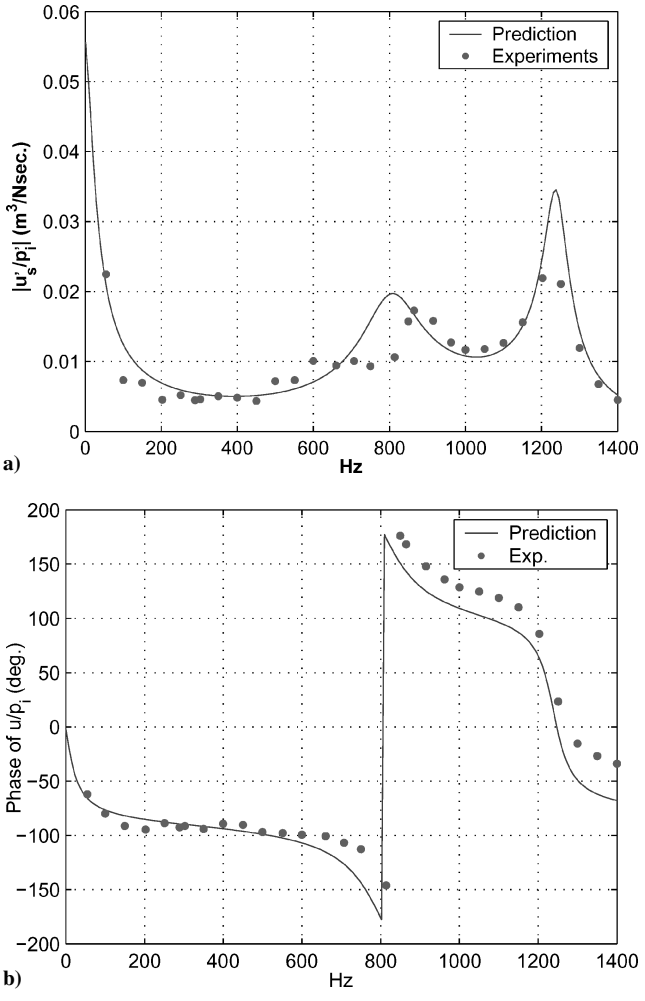


**Fig. 9 Comparison $u'_{ss}/p'_i$ of combined model and experiments with slot width $\delta = 0.813$ mm (0.032 in.) and tubing length $l_t = 0.152$ m (6 in.): a) magnitude and b) phase.**

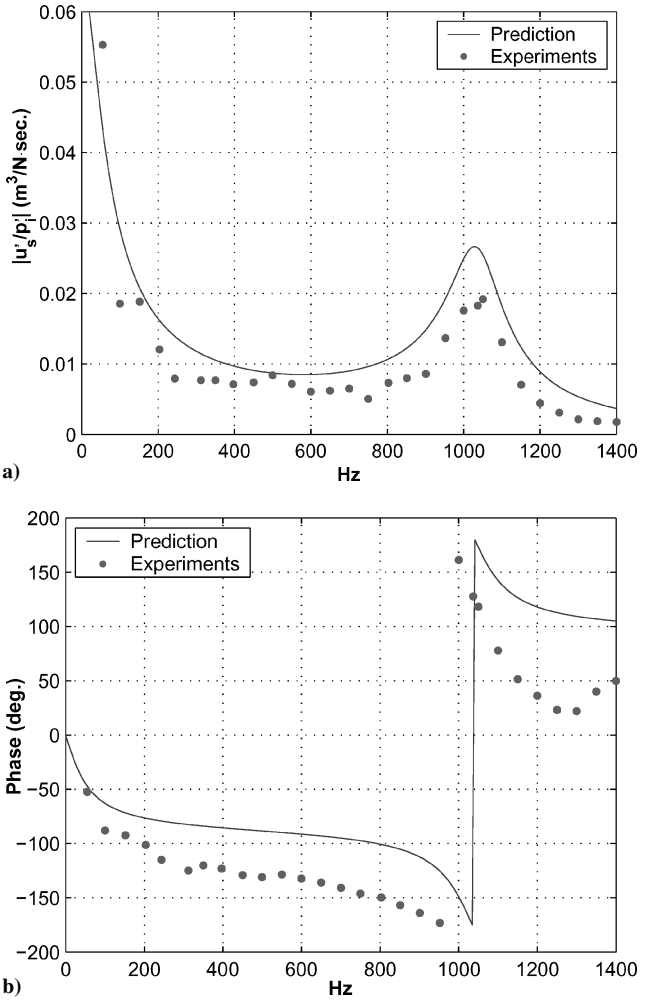


**Fig. 10 Comparison $u'_{ss}/p'_i$ of combined model and experiments with slot width $\delta = 0.813$ mm (0.032 in.) and tubing length $l_t = 0.051$ m (2 in.): a) magnitude and b) phase.**

amplitudes of $u'_s/p_i$' are similar to the amplitudes of $p'_r/p'_i$ in Fig. 7, but the velocity amplitudes steadily decrease as the frequency increases. The reduction in slot velocity amplitude is related to the increased impedance of oscillating flows through the slot. The impedance increase is primarily due to the increasing reactance ($j\omega L$) component. Note that when the pulsed-blowing system resonates with the tubing, the phase changes rapidly from $-90$ to 90 deg.

To quantify the comparison between the model and experiment, the standard deviations as a percentage of the local quantities were computed for the amplitudes and the resonant frequencies. For the longest tube, $l_t = 0.914$ m, shown in Fig. 8a, the magnitude and resonant-frequency standard deviations were 18 and 2%, respectively. The modeling error for the intermediate-length tube $l_t = 0.152$ m shown in Fig. 9a increased to a 29% standard deviation in magnitude and a 6% in the resonant frequency. The shortest length tube data in Fig. 10a showed deviations of 38% and 3% in magnitude and frequency. The results show that deviations between model and experiment increase as the tubing length decreases, which may be an indication that the one-dimensional flow approximation of the transmission model is breaking down.

The effect of the slot width on the exit velocity $u'_s/p'_i$ from the pulsed-blowing system is shown in Fig. 11. The tubing length was fixed at 0.381 m, so only the actuator impedance associated with changing the slot exit affects the combined model. Comparing Figs. 11a, 11b, and 11c, one can see that the dynamic response of the pulsed-blowing system changes with decreasing or increasing slot width. The largest influence of slot width on the amplitude distribution of $u'_s/p'_i$ occurs at frequencies above 600 Hz. The amplitude of the velocity fluctuation is affected by both the transmission tubing transfer function and the impedance of the actuator. For the particular tubing length used in this experiment, the intermediate slot width 0.813 mm produced the largest velocity amplitude at the resonant frequency of 400 Hz. This result illustrates the need to tune the actuator to the tubing in order to achieve the largest fluctuation levels.

## V. Discussion

It was shown in Fig. 7 that longer transmission tubes exhibited different frequency spacings between resonance peaks, depending on the forcing frequency. The change in frequency spacing between resonance peaks can be related to a change in resonance mechanism. The first resonance mechanism at lower frequencies can be described as having "open-end resonance" characteristics, in which the first resonance peak wavelength matches the half-wavelength of the tubing length. The second resonance mechanism can be described as having "closed-end resonance" characteristics. The tubing length will be one quarter of the wavelength for the first closed-end resonance. Unlike that for the open-end resonance, the second resonance frequency will be three times the first resonance frequency. This was observed at intermediate forcing frequencies, where irregular peak spacing was observed. At the highest forcing frequencies, the frequency spacing between peaks became uniform again with a difference between peaks that was close to the "open-end resonance" seen at low frequencies. The results illustrate the effect of a changing actuator impedance, which is the downstream boundary condition of the transmission tubing. Therefore, the frequency-dependent actuator impedance determines which resonance mechanism the pulsed blowing system will undergo. The reflection coefficient is a useful

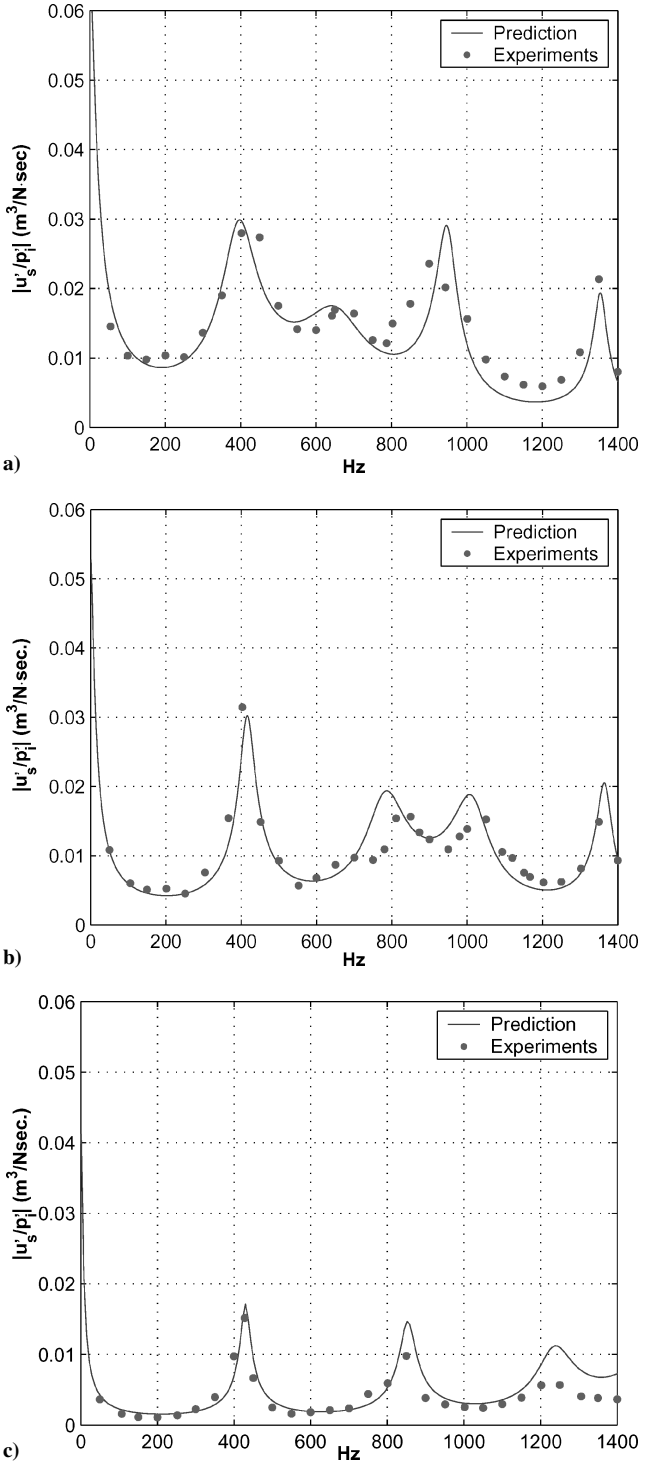


**Fig. 11 Effect of slot width on $u_s'/p_i'$, for tubing length $l = 0.381$ m (15 in.): a) slot width $\delta = 0.406$ mm (0.016 in.), b) $\delta = 0.813$ mm (0.032 in.), and c) $\delta = 2.16$ mm (0.085 in.).**

quantity for characterizing the actuator impedance, and is described next.

The reflection coefficient is defined as the ratio of the pressure of the reflected wave to the pressure of the incident wave at the receiving end of the line. In the pulsed-blowing systems, the pressure in the tube can be expressed as

$$p = \left(p_1 e^{\Gamma x} + p_2 e^{-\Gamma x}\right) e^{i\omega t} \tag{20}$$

where $p_1 e^{\Gamma x}$ is the incident wave that travels from the oscillatory valve to the load and $p_2 e^{-\Gamma x}$ is the reflected pressure wave that travels in the upstream direction. The reflected pressure wave forms at the end of a transmission line when the line is terminated in any impedance other than the characteristic impedance of the line $Z_o$.

The reflection coefficient can be expressed in terms of the impedance of the actuator $Z_r$ and the characteristic impedance of the tubing:

$$\zeta = p_2/p_1 = (Z_r - Z_o)/(Z_r + Z_o) \tag{21}$$

The reflection coefficient is a complex function of frequency. The real part of the reflection coefficient indicates whether the reflected

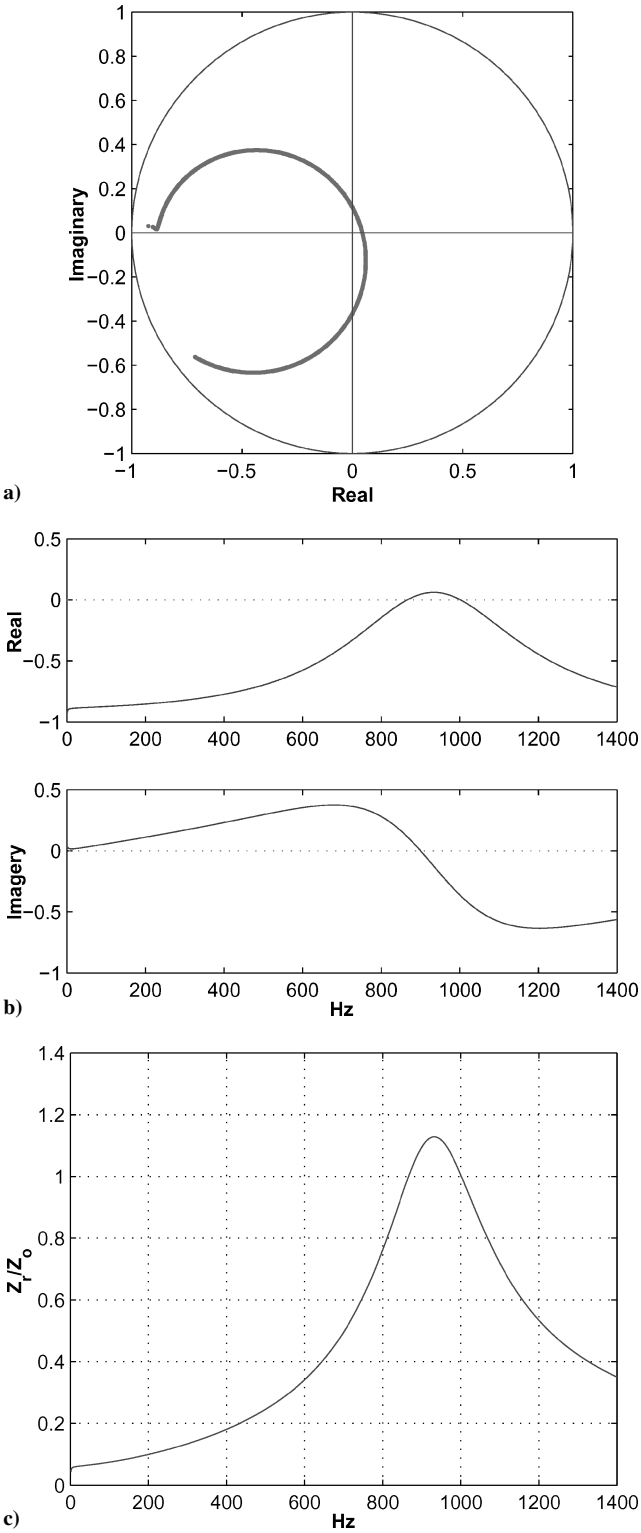


**Fig. 12 Impedance characteristics of the transmission tube for slot width $\delta = 0.813$ mm and tubing length $l_t = 0.940$ m shown as a) reflection coefficients, b) real and imaginary parts of reflection coefficient, and c) $Z_r/Z_o$ vs forcing frequency.**

wave will be a compression wave or an expansion wave relative to the incident compression wave. If the real part of the reflection coefficient is positive, then the signs of $p_2$ and $p_1$ have the same sign. For example, the compression wave reflects as a compression wave. The phase between the real and imaginary parts of the reflection coefficient indicates the phase between the incident compression and reflected waves. The magnitude of the reflection coefficient is bounded by one, because the reflected wave amplitude cannot be greater than that of the incident wave.

The behavior of the irregular peaks appearing in Fig. 7a between 800 Hz and 1 kHz can be explained by considering the reflection coefficient plots in Fig. 12. The magnitude of the actuator impedance depends on the resistance and inertance of the slot exit and the compliance of the actuator cavity, as shown in Eq. (15a). The impedance of the actuator $Z_r$ is frequency-dependent, and a maximum of $Z_r$ may exist in the forcing frequency range. Consequently, the impedance ratio $Z_r/Z_o$ also has a maximum at the frequency where the actuator impedance $Z_r$ is maximized. The impedance ratio $Z_r/Z_o$ corresponding to Fig. 7a has a maximum at 930 Hz as shown in Fig. 12c. When the frequency reaches 840 Hz, the impedance of the actuator $Z_r$ becomes greater than the characteristic impedance of the tube $Z_o$. Simultaneously the reflection coefficient becomes positive, as seen in Fig. 12a, and the tubing end resonance characteristic changes from open-end to closed-end resonance. The peaks at 873 and 987 Hz in Fig. 7a are characteristic of the closed-end resonance. It is for this reason that the frequency difference is 114 Hz between the two peaks at 873 and 987 Hz, which is much smaller than the 180-Hz frequency difference observed for the first four peaks. On the other hand, when the oscillating frequency exceeds 1000 Hz, the impedance of the actuator drops again and the system resonance characteristic changes back to open-end resonance. Note that $Z_r/Z_o$ drops quickly after 1000 Hz in Fig. 12c. The peaks generated at 1150 and 1324 Hz are in the state of open-end resonance again. The frequency difference of 174 Hz between the peaks is slightly less than the 180 Hz of the first four peaks, because of higher dissipative loss in the transmission tubing at higher frequencies.

The higher actuator impedance associated with the decreasing slot width explains the change of the system resonance that occurs at the lower forcing frequencies. As shown in Fig. 11, the impedance of the actuator decreases with increasing slot width from 0.406 mm (Fig. 11a) to 2.16 mm (Fig. 11c). The irregular spacing of the resonance peaks around 655 Hz observed with the smallest slot width in Fig. 11a does not appear in Fig. 11c over the frequency range up to 1400 Hz. The peak spacing irregularity is found at 800 and 1000 Hz with the intermediate slot width 0.813 mm shown in Fig. 11b.

When an increase in the velocity fluctuation amplitudes at the slot exit is needed, one instinctively increases the supply pressure to the valve. However, this increases both the mean pressure in the actuator and the mean velocity at the slot exit. The resistance of the actuator slot increases in proportion to the slot exit flow speed at high amplitudes,[17,18] which reduces the magnitude of $u_s'/p_i'$. A significant drop in the fluctuating velocity amplitude can be seen by comparing Fig. 13a with Fig. 13b, which correspond to the slot exit velocity increasing from $\bar{U}_s = 20$ m/s to $\bar{U} = 80$m/s. At very low mean pressures the velocity will be low; therefore some optimum mean velocity that maximizes the $u_s'/p_i'$ ratio will exist for a given pulsed-blowing system.

The results in Fig. 14 provide one additional example of the mean flow effect on the actuator transfer function. The ratios of the fluctuating slot exit velocity to the fluctuating pressures in the actuator cavity, $u_s'/p_r'$, were measured and compared to the predictions in

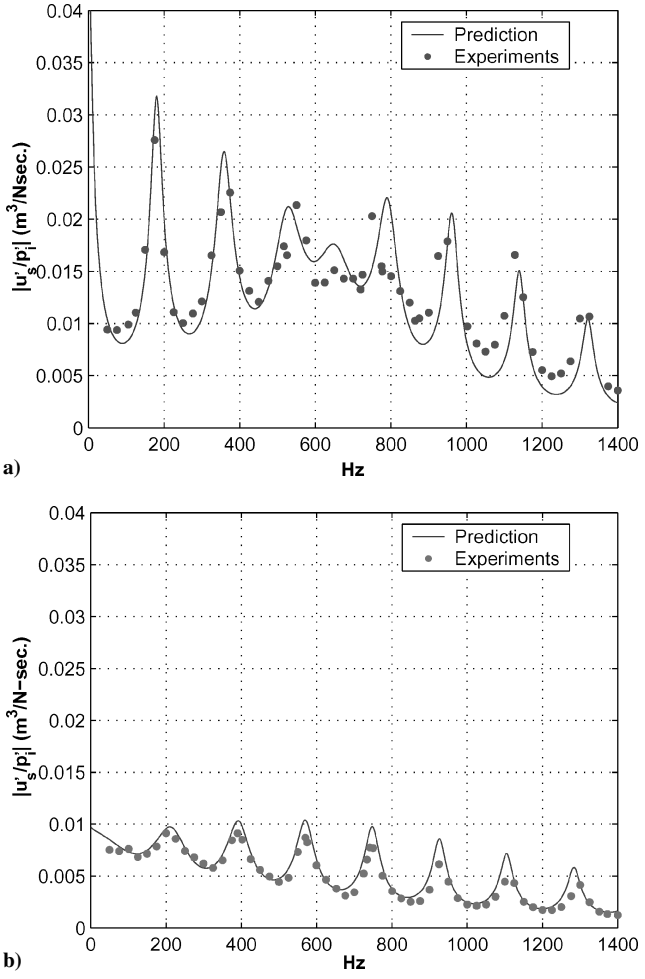


**Fig. 13 Effect of mean flow velocity on $u_s'/p_i'$, for $l = 0.914$ m (36 in.) and slot width $\delta = 0.406$ mm (0.016 in.): a) mean velocity $\bar{U} = 20$ m/s and b) $\bar{U} = 80$ m/s.**

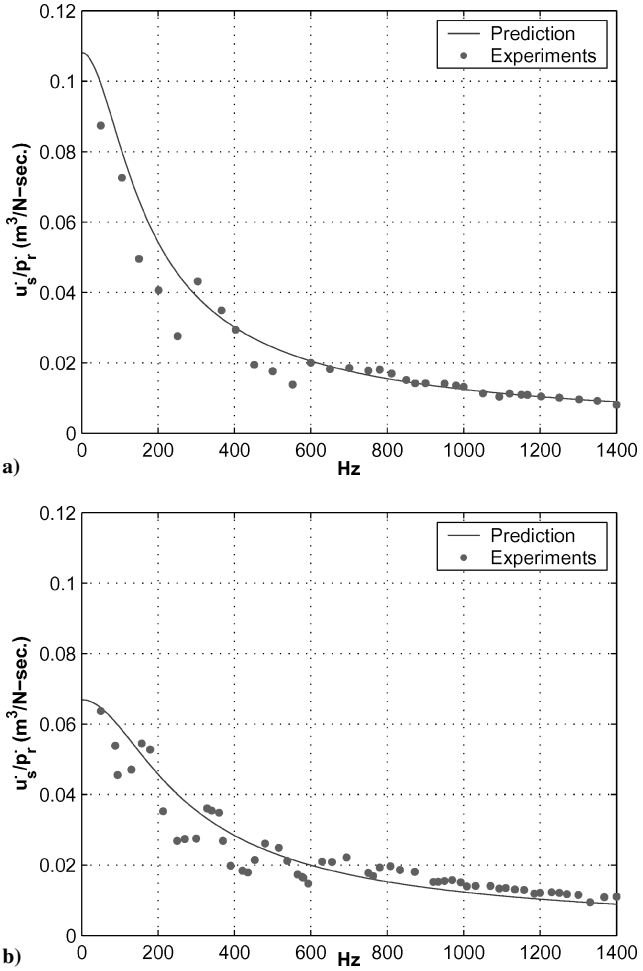


**Fig. 14 Effect of mean flow velocity on $u_s'/p_r'$ with slot width $\delta = 0.032$ in.: a) mean velocity $\bar{U} = 14$ m/s and b) $\bar{U} = 22$ m.**

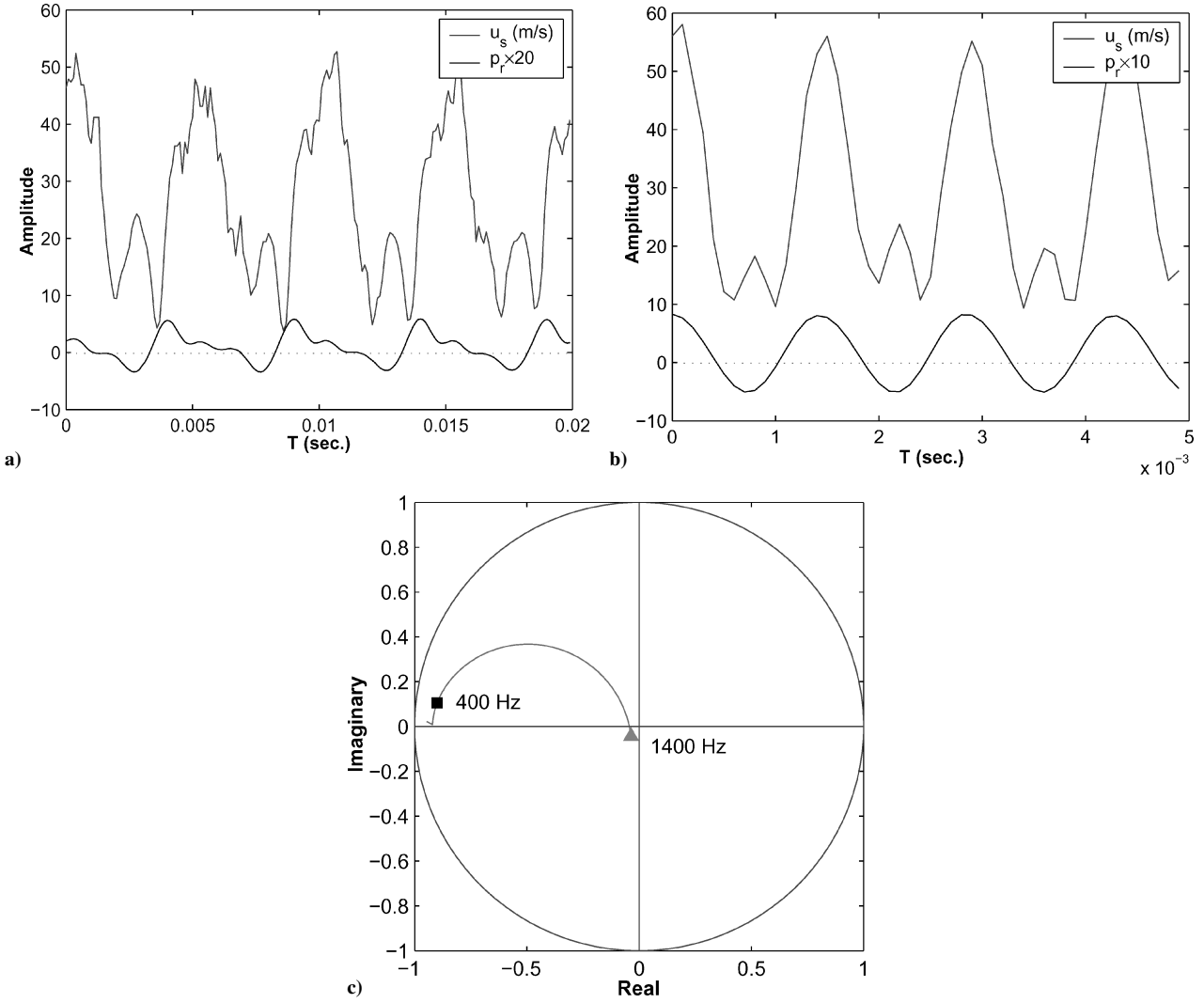


**Fig. 15 Time series slot exit velocity with slot width $\delta = 0.085$ in. and tubing length $l = 2$ in.: a) 400 Hz, b) 1400 Hz, and c) corresponding reflection coefficients.**

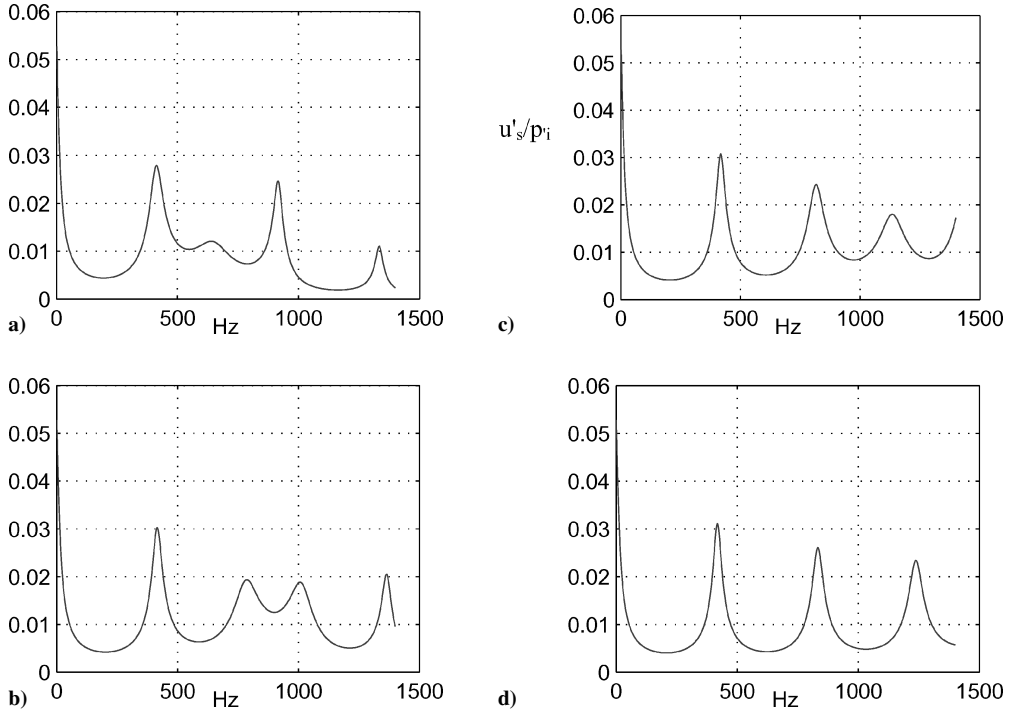


**Fig. 16 Effects of the actuator chamber volume (predictions) on $u_s'/p_i'$ with slot width = 0.813 mm, and $l_t = 0.381$ m: a) $2.02 \times 10^{-5}$ m$^3$, b) $1.01 \times 10^{-5}$ m$^3$, c) $0.606 \times 10^{-5}$ m$^3$, and d) $0.202 \times 10^{-5}$ m$^3$.**

Fig. 14. The actuator transfer function $u'_s/p'_r$ also drops significantly after the mean velocity is increased from $\bar{U} = 14$ m/s (Fig. 14a) to $\bar{U} = 22$ m/s (Fig. 14b). Again, the increasing mean flow velocity through the slot increases the acoustic resistance, so that the acoustic resistance of the mean velocity $\bar{U} = 22$ (m/s) in Fig. 14b is much higher than that of $\bar{U} = 14$ (m/s) shown in Fig. 14a.

Under certain forcing conditions it is possible for the fluctuating velocity amplitude to exceed the mean velocity at the actuator exit, which creates a flow reversal during part of the cycle in the pulsed blowing actuator. This behavior is one example of a counterintuitive result that can occur with a pulsed blowing actuator. The reversed flow phenomenon can be seen in the time series of the velocity at the actuator slot $u_{s,}$ shown in Fig. 15.

The reflection coefficient can be used to predict when reversed flow is possible. When the real part of the reflection coefficient is negative, an expansion wave is produced at the slot exit as the incident compression wave leaves the slot exit. If the expansion wave is sufficiently strong the instantaneous pressure drops below the mean pressure, and the pressure decreases even further below the ambient pressure for a portion of the cycle of oscillations. Simultaneously, the fluctuating velocity exceeds the mean velocity and causes a reversed flow at the slot exit. This behavior is shown with the forcing frequency of 400 Hz in Fig. 15a and 1400 Hz in Fig. 15b. The hot-wire signal from a probe placed slightly above the exit plane of the actuator slot is rectified during the time that the pressure signal is negative. The real parts of the reflection coefficients for both cases are negative, as shown in Fig. 15c.

A final example of unexpected behavior in pulsed blowing systems is associated with changes in the actuator volume. There is a common misconception that increasing the volume between the oscillating valve and the actuator always decreases the velocity output amplitude. Figure 16 shows the predictions of the transfer function, $u'_s/p'_i$ with four different actuator cavity volumes. The peak at 415 Hz gradually increases when the actuator volume is decreased. However, note that the peak at 915 Hz in Fig. 16a also reaches $u'_s/p'_i = 0.0245$, which is comparable to the peaks in other cases where the cavity volume is smaller. The results presented in this study show a more complicated situation in which the presence of the volume actually enhances the oscillation amplitude at resonant conditions. Therefore, generalizations about the effect of geometry on fluctuation levels must be made with great care.

## VI. Conclusions

The behavior of a pulsed-blowing system consisting of an oscillating valve, long tubing, and an actuator was modeled with an electroacoustic analog and studied experimentally. Model validation experiments were conducted with a setup that simulated a pulsed blowing system connected to a compressor stator. A distributed model for the tubing was combined with a lumped-element model of the actuator to simulate the overall system. The results show the complexity of the pulsed-blowing system behavior and the importance of a model for guiding the system design.

The transfer functions of $p'_r/p'_i$, $u'_s/p'_i$, and $u'_s/p'_r$ were obtained from the model and experimental measurements. The results demonstrate that the pulsed-blowing system performance is strongly dependent on the geometry (tubing length, slot widths, and volume of the cavity), forcing frequencies, and exit flow velocity amplitudes. The combined model predicted the resonant frequencies to within 10% and the amplitudes of the velocity at the exit of the actuator to within 40%. Comparisons between the model and experiment improved as the transmission tubing lengths increased.

Some examples of counterintuitive phenomena were observed under certain operating conditions. At resonant conditions the pressure oscillation amplitudes at the entrance to the actuator and inside the actuator cavity could be substantially higher than the mean pressure, which resulted in reversed flow at the actuator exit for a portion of the forcing cycle. Reversed flow could occur when the real part of the reflection coefficient was negative and the fluctuating velocity exceeded the mean velocity amplitude. It was also seen that increasing the system pressure does not always increase the fluctuation amplitude, and reducing cavity volume does not necessarily increase peak amplitudes. These observations underscore the importance of modeling both the transmission tube and the actuator when designing a pulsed-blowing flow control system.

## Acknowledgments

Support for the Honeywell Smartvane project is through the Defense Advanced Research Projects Agency Microadaptive Flow Control program managed by Rich Wlezien and Steven Walker and administered through the Army Research Office by Tom Doligalski. Support for B.-H. Kim was provided by Aerospace Illinois, a NASA Space Grant consortium. The cooperation of Tony Strazisar, Michelle Bright, and Dennis Culley at NASA Glenn Research Center during the development of the model is appreciated.

## References

[1]Williams, D. R., Acharya, M., Bernhardt, J., and Yang, P., "The Mechanism of Flow Control on a Cylinder with the Unsteady Bleed Technique," AIAA Paper 91-0039, Jan. 1991.

[2]Amitay, M., Smith, B. L., and Glezer, A., "Aerodynamic Flow Control Using Synthetic Jet Technology," AIAA Paper 98-0208, Jan. 1998.

[3]Smith, D. R., Amitay, M., Kibens, V., Parekh, D. E., and Glezer, A., "Modification of Lifting Body Aerodynamics Using Synthetic Jet Actuators," AIAA Paper 98-0209, Jan. 1998.

[4]Seifert, A., Eliahu, S., Greenblatt, D., and Wygnanski, I., "Use of Piezoelectric Actuators for Airfoil Separation Control," *AIAA Journal*, Vol. 36, No. 8, 1998, pp. 1535–1537.

[5]Chen, Y., Liang, S., Aung, K., Glezer, A., and Jagoda, J., "Enhanced Mixing in a Simulated Combustor Using Synthetic Jet Actuators," AIAA Paper 99-0449, Jan. 1999.

[6]Smith, B. L., and Glezer, A., "The Formation and Evolution of Synthetic Jets," *Physics of Fluids*, Vol. 10, No. 9, 1998, pp. 2281–2297.

[7]Rathnasingham, R., and Breuer, K. S., "Coupled Fluid–Structural Characteristics of Actuators for Flow Control," *AIAA Journal*, Vol. 35, No. 5, 1997, pp. 832–837.

[8]McCormick, D. C., "Boundary Layer Separation Control with Directed Synthetic Jets," AIAA Paper 2000-0519, Jan. 2000.

[9]Gallas, Q., Holman, R., Nishida, T., Carroll, B., Sheplak, M., and Cattafesta, L., "Lumped Element Modeling of Piezoelectric-Driven Synthetic Jet Actuators," *AIAA Journal*, Vol. 41, No. 2, 2003, pp. 240–247.

[10]Beranek, L. L., *Acoustics*, Acoustical Society of America, Cambridge, MA, 1993, pp. 47–77, 116–143.

[11]Fischer, J., *Fundamentals of Electroacoustics*, Interscience, New York, 1955, Chaps. 3 and 11.

[12]Rohmann, C. P., and Grogan, E. C., "On the Dynamics of Pneumatic Transmission Lines," *Transactions of the American Society of Mechanical Engineers*, Vol. 79, May 1957, pp. 853–874.

[13]Karam, J. T., and Franke, M. E., "The Frequency Response of Pneumatic Lines," *Journal of Basic Engineering*, Vol. 90, No. 2, 1967, pp. 371–378.

[14]Nichols, N. B., "The Linear Properties of Pneumatic Transmission Lines," *Transactions of the Instrument Society of America*, Vol. 1, No. 1, 1962, pp. 5–14.

[15]Iberall, A. S., "Attenuation of Oscillatory Pressures in Instrument Lines," *Journal of Research of the National Bureau of Standards*, Vol. 45, July 1950, pp. 85–108.

[16]Ingard, U., "On the Theory and Design of Acoustic Resonators," *Journal of the Acoustical Society of America*, Vol. 25, Nov. 1953, pp. 1037–1061.

[17]Ingard, U., and Ising, H., "Acoustic Nonlinearity of an Orifice," *Journal of the Acoustical Society of America*, Vol. 42, No. 1, 1967, pp. 6–17.

[18]Thurston, G. B., Hargrove, L. E., and Cook, B. D., "Nonlinear Properties of Circular Orifices," *Journal of the Acoustical Society of America*, Vol. 29, No. 9, 1957, pp. 992–1001.

[19]Seifert, A., and Pack, L. G., "Oscillatory Control of Separation at High Reynolds Numbers," *AIAA Journal*, Vol. 37, No. 9, 1999, pp. 1062–1071.

[20]Skilling, H. H., *Electric Transmission Lines*, Krieger, New York, 1979, pp. 1–93.

[21]Tijdeman, H., "On the Propagation of Sound Waves in Cylindrical Tubes," *Journal of Sound and Vibration*, Vol. 39, July 1975, pp. 1–33.

M. Ahmadian
*Associate Editor*